Available online at www.sciencedirect.com
SCIENCE DIRECT®
Chemical Physics 315 (2005) 41–52
Chemical Physics
www.elsevier.com/locate/chemphys

Infrared spectroscopic detection of the methylsilyl (CH_3SiH_2, X^2A') and the silylmethyl (CH_2SiH_3, X^2A') radicals and their partially deuterated counterparts in low temperature matrices

David S. Sillars [a], Chris. J. Bennett [a], Yoshihiro Osamura [b], Ralf I. Kaiser [a,*]

[a] *Department of Chemistry, University of Hawai'i at Manoa, Honolulu, HI 96822, USA*
[b] *Department of Chemistry, Rikkyo University, 3-34-1 Nishi-ikebukuro, Tokyo 171-8501, Japan*

Received 6 December 2004; accepted 4 February 2005
Available online 26 April 2005

Abstract

Both the methylsilyl, $CH_3SiH_2(X^2A')$, and the silylmethyl, $SiH_3CH_2(X^2A')$, together with their partially deuterated isotopomers were identified for the first time via infrared spectroscopy in low temperature silane–methane matrices at 10 K upon exposure of the matrices with mono energetic electrons. Three fundamentals at 654 cm^{-1} (ν_8), 1414 cm^{-1} (ν_{12}), and 1251 cm^{-1} (ν_5) (methylsilyl) and one absorption at 645 cm^{-1} (ν_8) (silylmethyl) were detected; these assignments were confirmed by identifying also partially deuterated radicals through their absorptions at 781 cm^{-1} (ν_7), 1415 cm^{-1} (ν_{12}), 1419 cm^{-1} (ν_4), and 1546 cm^{-1} (ν_{11}) (d2-methylsilyl, CH_3SiD_2) and 582 cm^{-1} (ν_8), 749 cm^{-1} (ν_5), and 771 cm^{-1} (ν_{13}) (d3-silylmethyl, SiD_3CH_2) in d4-silane–methane matrices. Since both silane and methane have been observed in the circumstellar envelope of the carbon star IRC+10216, our investigations assist in future infrared spectroscopic, astronomical searches for these species in interstellar space. Likewise, the knowledge of the infrared absorption features might help to follow the chemical evolution of organo-silicon CVD process via time resolved infrared spectroscopy.

1. Introduction

Small, binuclear organosilane molecules and their radicals of the generic formula $SiCH_x$ ($x = 1$–6) are important precursors to prepare amorphous silicon carbide (a-Si–C) films via chemical vapor deposition (CVD) [1,2]. The fully dehydrogenated silicon monocarbide (SiC) is considered as a promising class of materials for high temperature and high power electronic devices since silicon carbide is chemically and mechanically inert and presents a wide-band gap (2.2–2.3 eV) semiconductor [3,4]. In the early years, amorphous silicon carbide films were produced via chemical vapor deposition of mixtures of silicon and carbon bearing gases such as silane (SiH_4) and methane (CH_4) [5,6]. Due to the strong carbon–hydrogen bond in the methane molecule, this approach required excessive growth temperatures, often inducing high tensile stress in the silicon carbide films. Recently, the use of single precursor molecules such as methylsilane, CH_3SiH_3, has been exploited successfully [7,8]. However, to optimize and even to manipulate the nucleation processes, it is crucial to understand the fundamental, underlying chemical mechanisms in depth. Reaction networks which actual model the chemical vapor deposition processes of organo silanes [9,10] demand crucial input parameters. These are rate constants of the critical reactions involved, the reaction intermediates together with the final reaction products, and their thermochemical data [11–17].

An understanding of the energetics and spectroscopic properties of simple silicon–carbon bearing species is

* Corresponding author. Fax: +1 808 956 5908.
E-mail address: kaiser@gold.chem.hawaii.edu (R.I. Kaiser).

0301-0104/$ - see front matter © 2005 Elsevier B.V. All rights reserved.
doi:10.1016/j.chemphys.2005.02.011

also of crucial importance to untangle the elementary chemical reactions involved in circumstellar envelopes of dying carbon stars. About 15% of the observed interstellar molecules contain silicon ranging from simple diatomics (SiC, SiN, SiO, SiS), triatomics (SiCN) and a silicon-terminated cummulene (CCCCSi) to two cyclic species (SiC_2, SiC_3) [18,19]. Here, the silane and methane molecules – precursors to more complex organo silicon molecules – have been detected in the outflow of carbon stars [20].

However, despite the importance of the organosilyl molecules as rate limiting growth species of a-Si–C films in chemical vapor deposition processes and their astrophysical potential to form silicon carbide molecules, the vibration levels of the corresponding radicals have not been investigated experimentally. Here, a detailed knowledge of the infrared absorption features might help to follow the chemical evolution of CVD processes in real time not only via mass spectrometry [4], but also through time resolved infrared spectroscopy. Here, the methylsilane (CH_3SiH_3; $\Delta H_f^0 = -31$ kJ mol^{-1}) molecule as well as the corresponding silylmethyl CH_2SiH_3 ($\Delta H_f^0 = 174$ kJ mol^{-1}) and methylsilyl CH_3SiH_2 ($\Delta H_f^0 = 139$ kJ mol^{-1}) doublet radicals have received particular attention [21,22]. The spectroscopic properties of the methylsilane molecule (CH_3SiH_3) have been studied extensively [23], and both microwave [24–27] as well as infrared spectra [28,29] are well known. The bond distances have been determined to be 109.6 nm (CH bond), 148.3 nm (Si–H bond), and 186.9 nm (Si–C bond); the H–C–Si and H–Si–C bond angles were calculated to be 110.9° and 110.5°, respectively. The $SiCH_5$ radicals are thought to be the key intermediates in the growth of amorphous silicon carbide films. A theoretical study of CVD processes utilizing an ethylsilane ($C_2H_5SiH_3$) precursor suggests that the CH_2SiH_3 species can be formed via a barrier-less methyl radical loss pathway; this process was calculated to be endothermic by 330 kJ mol^{-1}[30] and 371 kJ mol^{-1} [31]. Recently, the CH_2SiH_3 and CH_3SiH_2 radicals were proposed to be formed via methylidene (CH) insertion into a silicon–hydrogen bond of silane and silylidene (SiH) insertion into a carbon–hydrogen bond of methane [32]; both reactions are barrier-less. Alternatively, kinetic studies in the temperature range of 291–1360 K suggest that hydrogen atoms can abstract a hydrogen atom from the methylsilane molecule (CH_3SiH_3) via a barrier of about 11 kJ mol^{-1}; however, the nature of the $SiCH_5$ isomer could not be identified since the experiments only follow the decay kinetics of the atomic hydrogen reagent [33–35]. Guided ion beam studies suggest that the enthalpy of formation of the CH_3SiH_2 radical ranges between 130 and 160 kJ mol^{-1} [36]. Note that solely the CH_3SiH_2 radical was observed in a matrix via ESR at 77 K as a reaction product of vibrationally excited methyl radicals via hydrogen abstraction from neighboring CH_3SiH_3; the CH_2SiH_3 isomer is thermodynamically less stable by 41 kJ mol^{-1} and was not observed [37]. Note that a ^{60}Co γ irradiation of methylsilane yielded solely the energetically preferred CH_3SiH_2 radical [38,39]. Similar to the methylsilane molecule, the infrared [40,41] and millimeter spectra [42] of the closed shell H_2CSiH_2 species are also known; various theoretical investigations have been carried out on the $SiCH_4$ potential energy surfaces as well [43,44]. Smaller, hydrogenated silicon–carbon clusters have been investigated, too. For instance, the vibrational levels of the $H_2CSiH(^2A')$ and $CH_3Si(^2A'')$ isomers have been determined via negative ion photoelectron spectroscopy [45]. Smith et al. assigned the fundamentals of $H_2CSi(^1A_1)$ via wavelength resolved fluorescence and stimulated emission pumping (SEP) [46]. The rearrangement to the $HCSiH(^1A')$ and $CSiH_2(^1A_1)$ isomers has also been probed theoretically [47,48]. Likewise, the vibrational levels and rovibronic spectra of $HCSi(^2\Sigma_g)$ have been recorded in the gas phase [49,50]. A recent matrix isolation study determined the ν_1 mode of the HCSi radical to be at 1010 cm^{-1} [51]; this measurement is in close agreement with the gas phase value of 1013 cm^{-1} [52] and a theoretical investigation [53].

Despite the importance of the $SiCH_x$ species in chemical vapor deposition processes and in the chemistry of circumstellar envelopes, the infrared spectroscopic properties of the $SiCH_5$ radicals are still elusive. This is of particular importance to identify structural isomers and open shell radicals which are thought to be essential growth species in CVD and circumstellar environments. In this paper, we present a combined experimental and theoretical study on the $SiCH_5$ radical and elucidate for the first time the position of the most intense, hitherto elusive infrared absorption frequencies of the methylsilyl and silylmethyl isomers together with their partially deuterated counterpart in low temperature silane–methane matrices. We demonstrated earlier that an interaction of energetic electrons can cleave a carbon–hydrogen bond in a methane molecule to form atomic hydrogen and a methyl radical at 10 K, reaction (1). Two neighboring methyl radicals were found to recombine forming an ethane molecule (2) [54]. Upon further irradiation with electrons, the ethane molecule decomposes to a hydrogen atom plus an ethyl radical, Eq. (3). In a similar manner, the dilsilyl (Si_2H_5) radical was synthesized in low temperature silane matrices (reactions (4)–(6)) [55]. Here, we export this concept and attempt to synthesize two $SiCH_5$ radical isomers via a homologous reaction sequence involving a cross recombination of a methyl with a silyl radical, followed by an atomic hydrogen loss (reactions (7) and (8))

$$CH_4(X^1A_1) \rightarrow CH_3(X^2A_2'') + H(^2S_{1/2}) \quad (1)$$

$$CH_3(X^2A_2'') + CH_3(X^2A_2'') \rightarrow C_2H_6(X^1A_{1g}) \quad (2)$$

$$C_2H_6(X^1A_{1g}) \rightarrow C_2H_5(X^2A') + H(^2S_{1/2}) \quad (3)$$

$$SiH_4(X^1A_1) \rightarrow SiH_3(X^2A_1) + H(^2S_{1/2}) \quad (4)$$

$$SiH_3(X^2A_1) + SiH_3(X^2A_1) \rightarrow Si_2H_6(X^1A_{1g}) \quad (5)$$

$$Si_2H_6(X^1A_{1g}) \rightarrow Si_2H_5(X^2A') + H(^2S_{1/2}) \quad (6)$$

$$SiH_3(X^2A_1) + CH_3(X^2A_2'') \rightarrow CH_3SiH_3(X^1A_1) \quad (7)$$

$$CH_3SiH_3(X^1A_1) \rightarrow CH_3SiH_2/CH_2SiH_3(X^2A') + H(^2S_{1/2}). \quad (8)$$

2. Experimental

The experiments were carried out in a contamination-free ultrahigh vacuum (UHV) setup consisting of a 15 l cylindrical stainless steel chamber of 250 mm diameter and 300 mm height; this system can be evacuated down to 8×10^{-11} Torr by a magnetically suspended turbo-pump backed by an oil-free scroll pump [56]. A rotatable, two stage closed cycle helium refrigerator is attached to the lid of the machine and holds a polished silver mono crystal. This crystal is cooled to 10.2 ± 0.3 K and serves as a substrate for the silane–methane ices. The ices were prepared at 10 K by depositing silane (99.99%) and methane (99.99%) at pressures of 8×10^{-8} Torr for 20 min onto the cooled silver crystal. Fig. 1 shows a typical infrared spectrum of the frost at 10 K; all absorptions are summarized in Table 1.

To determine the ice composition and thickness, we integrated the infrared absorption features at 2164 and 883 cm^{-1} (silane) as well as 4200, 3852, and 2815 cm^{-1} (methane). The ice thicknesses are then calculated via the Lambert–Beers relationship [56]. Considering the integrated absorption coefficients of these fundamentals,

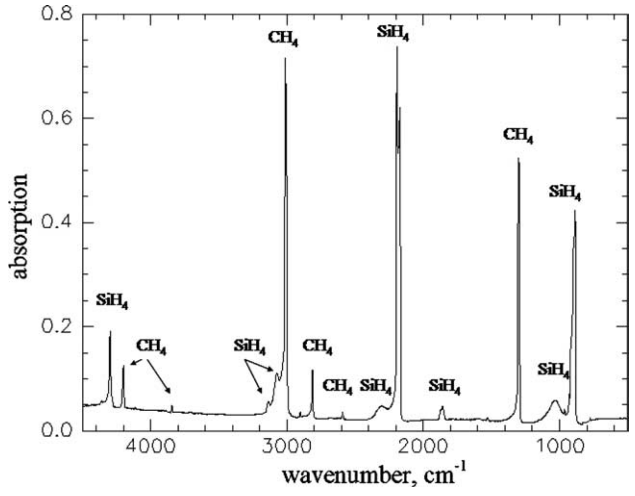

Fig. 1. Infrared spectrum of the silane–methane frost at 10 K. The assignments of the peaks are compiled in Table 1.

Table 1
Infrared absorptions of the silane–methane ices and their assignments

Frequency (cm^{-1})	Assignment	Molecule	Frequency (cm^{-1})
4523	$\nu_2 + \nu_3$	CH_4	4527
4364	$2\nu_3$	SiH_4	4354
4358	$\nu_3 + \nu_4$	CH_4	4349
4298	$\nu_3 + \nu_4$	CH_4	4283
4292	$\nu_1 + \nu_3$	SiH_4	4283
4200	$\nu_1 + \nu_4$	CH_4	4200
4112	$\nu_2 + 2\nu_4$	CH_4	4113
3852/3895	$3\nu_4$	CH_4	3891/3851
–	$\nu_3 + \nu_4 + \beta$	SiH_4	3142 (sh)
3139	$\nu_2 + \nu_3$	SiH_4	3128
–	$\nu_3 + \nu_4 + \alpha$	SiH_4	3087
3074	$\nu_3 + \nu_4$	SiH_4	3060
3011	ν_3	CH_4	3000
2815	$\nu_2 + \nu_4$	CH_4	2815
2595	$2\nu_4$	CH_4	2595
2306	$\nu_3 + \gamma$	SiH_4	2300
–	$\nu_3 + \beta$	SiH_4	2250
2193	$\nu_3 + \alpha$	SiH_4	2195
2164	ν_3	SiH_4	2163
1878	$\nu_2 + \nu_4 + \alpha$	SiH_4	1876
1300	ν_4	CH_4	1293
1032	$\nu_2 + \beta/\nu_4 + \gamma$	SiH_4	1050
1032	$\nu_2 + \beta/\nu_4 + \gamma$	SiH_4	1050
961	ν_2	SiH_4	957
930	$\nu_4 + \beta$	SiH_4	948
914	$\nu_4 + \alpha$	SiH_4	918
883	ν_4	SiH_4	876

α, β, and γ denote lattice modes of the silane sample; the peak positions in the pure methane and silane samples are shown in column four for comparison [55].

i.e., 2.5×10^{-17} cm and 2.0×10^{-17} cm (silane) as well as 1.6×10^{-18} cm, 2.0×10^{-19} cm, and 2.3×10^{-18} cm (methane), this gives column densities of $2.0 \pm 0.1 \times 10^{17}$ cm^2 and $1.5 \pm 0.2 \times 10^{17}$ cm^2, respectively. Taking the densities of the silane and methane ices to 0.77 ± 0.03 and 0.53 ± 0.02 g cm^{-3} [57], this translates into thicknesses of 140 ± 15 nm silane and 70 ± 20 nm methane, respectively. To confirm the assignments of the methylsilyl and silylmethyl radicals we also conducted irradiations of d4-silane–methane mixtures at 10 K (SiD_4:$CH_4 = 1.3 \pm 0.1$:1; thicknesses: 130 ± 10 nm d4-silane and 65 ± 10 nm methane).

To understand the fine structure of the infrared features of the binary ice mixture, it is important to comment briefly on the modifications of the pure solids. At 10 K, methane ice exists in a low-temperature cubic phase II. The carbon atoms of the methane molecules form a cubic close-packed structure for each octant; each unit cell has a lattice constant $a_0 = 11.68$ Å and contains 32 methane molecules [58]. This results in a well-defined fine structures and lattice vibrations ($\nu_L = 56 \pm 2$ cm^{-1}) superimposed on the ν_3 and ν_4 fundamentals at $\nu_3 + \nu_L = 3058$ cm^{-1} and $\nu_4 + \nu_L = 1348$ cm^{-1}. At 10 K, silane crystallizes in a tetragonal unit cell ($a_0 = b_0 = 12.5$ Å; $c_0 = 14.2$ Å) which contains 32 silane molecules [59]. The infrared spectrum of

crystalline silane shows distinct lattice modes (Table 1). We can compare this information with the infrared spectrum of the binary ice mixture (Fig. 1 and Table 1). Here, the lattice vibration of the methane crystal is not present. On the other hand, the α, β, and γ lattice modes of silane are still visible. This suggests that we have a solid solution of methane in silane; considering the similar lattice constants, each silane molecule can be replaced by a methane molecule. However, the visible lattice modes of silane indicate that we still have isolated regions of silane crystals in our solid ices. All together, these data imply an overall excess of silane compared to methane in our binary ices; this has been confirmed experimentally finding that the ratio of silane versus methane column densities is 1.3 ± 0.2.

Our ices were irradiated at 10 K with 5 keV electrons generated in an electron gun at beam currents of 100 nA by scanning the electron beam over an area of $3.0 \pm 0.4\ \mathrm{cm}^2$. Accounting for irradiation times of 60 min and the extraction efficiency of 78.8% of the electrons, this exposes the target to 1.8×10^{15} electrons. To guarantee an identification of the reaction products in the ices and those subliming into the gas phase on line and in situ, a Fourier transform infrared spectrometer (FTIR; solid state) and a quadrupole mass spectrometer (QMS; gas phase) were utilized. The Nicolet 510 DX FTIR spectrometer ($5000–500\ \mathrm{cm}^{-1}$) operates in an absorption–reflection–absorption mode (reflection angle $\alpha = 75°$). The infrared beam is coupled via a mirror flipper outside the spectrometer, passes through a differentially pumped potassium bromide (KBr) window, is attenuated in the ice sample prior and after reflection at a polished silver waver, and exits the main chamber through a second differentially pumped KBr window before being monitored via a liquid nitrogen cooled detector. The gas phase is monitored by a quadrupole mass spectrometer (Balzer QMG 420; 1–200 amu mass range) with electron impact ionization of the neutral molecules in the residual gas analyzer mode.

3. Theoretical approach

We have employed the hybrid density functional B3LYP method [60] with the 6-311G(d,p) basis functions in order to obtain the optimized structures and vibrational frequencies for $SiCH_x$ ($x = 5, 6$) systems. The relative energies are calculated by using the coupled cluster CCSD(T) method [61,62] with the aug-cc-pVTZ basis functions [63] at the structures obtained by the B3LYP method with the correction of B3LYP zero-point vibrational energies without scaling. All calculations were carried out with GAUSSIAN 98 program package [64]. In order to analyze the infrared spectra for the species obtained by present experiments, we have also calculated the vibrational frequencies and infrared intensities for the CH_3SiH_3, CH_3SiH_2, CH_2SiH_3, and for the partially deuterated species as shown in Table 2.

4. Computational results

Fig. 2 shows the optimized structures of $SiCH_6$ and $SiCH_5$ systems. The staggered conformation of CH_3SiH_3 is located at the energy minimum; the eclipsed conformation is the transition state of internal rotation around the carbon–hydrogen bond. This energy barrier of 6 kJ mol^{-1} is much smaller than the rotation barrier around the carbon–carbon bond in ethane. The structure $CH_3SiH_2(X^2A')$ is very similar to the structure of methylsilane. Since the bond strength of Si–H is weaker than that of C–H bond, the $CH_3SiH_2(X^2A')$ isomer calculated with CCSD(T) method is shown to be 39 kJ mol^{-1} more stable than the $CH_2SiH_3(X^2A')$ isomer. This energy difference is smaller than the values obtained with previous Hartree–Fock [65] and MP2 [66] calculations, but is excellent agreement with the experimental value of 37 kJ mol^{-1}. While the SiH_2 moiety of methylsilyl radical $CH_3SiH_2(X^2A')$ maintains nonplanarity, the radical center of silylmethyl $CH_2SiH_3(X^2A')$ has a sp^2 hybridized carbon; a gentle conjugation between p-orbital of carbon atom and Si–H bond makes C–Si bond (1.850 Å) slightly shorter than that of CH_3SiH_2 (1.885 Å) species. The structure of the planar sp^2 hybridized conformation of the SiH_2 moiety of methylsilyl radical is shown to be the transition state of the inversion of the SiH_2 and its energy barrier is calculated to be 26 kJ mol^{-1}. Note that we were unable to locate any hydrogen-bridged structure which presents a local minimum on the potential energy surface of $SiCH_5$ system. Both methylsilyl and silylmethyl radicals are connected via a transition state of the hydrogen migration as shown in Fig. 2 located 194 kJ mol^{-1} above the methylsilyl radical. This barrier height correlates nicely with a previous calculation of 178 kJ mol^{-1} and an experimental study of 171 kJ mol^{-1} [65]. Note that the energy barrier of internal rotation of methylsilyl and silylmethyl radicals are smaller than that of methylsilane. The eclipsed conformation of methylsilyl radical is less stable by 4 kJ mol^{-1} than the staggered conformer, while there is no energy difference between staggered and eclipsed conformations in the silylmethyl radical.

Also, we calculated the energetics for the reactions with the CCSD(T) method, summarized in Fig. 3 (the corresponding B3LYP energies are given in parentheses). The dissociation of the methane and silane molecules into the corresponding methyl and silyl radicals plus atomic hydrogen according to Eqs. (1) and (4) was calculated to be endoergic by 371 (370) kJ mol^{-1} and 427 (428) kJ mol^{-1}. The recombination of the methyl with the silyl radical is barrier-less and exoergic by 353

Table 2
Unscaled vibrational frequencies (cm^{-1}) and infrared intensities (cm molecule^{-1}) of CH_3SiH_3, CH_3SiD_3, CH_3SiH_2, CH_3SiD_2, CH_2SiH_3, and CH_2SiD_3 calculated with B3LYP/6-311G(d,p) level of theory

Mode		Characterization	Frequency	Intensity	Frequency	Intensity
			Staggered CH_3SiH_3		Staggered CH_3SiD_3	
ν_1	a_1	CH_3 sym. stretch	3031	1.10E − 18	3032	1.10E − 18
ν_2	a_1	SiH_3 sym. stretch	2221	1.15E − 17	1581	7.30E − 18
ν_3	a_1	CH_3 umbrella	1305	2.49E − 18	1304	1.89E − 18
ν_4	a_1	SiH_3 umbrella	949	3.95E − 17	736	2.19E − 17
ν_5	a_1	C–Si stretch	690	1.79E − 18	646	2.84E − 18
ν_6	a_2	Torsion	194	0.00E + 00	178	0.00E + 00
ν_7	e	CH_3 asym. stretch	3105	3.54E − 18	3105	1.69E − 18
ν_8	e	SiH_3 asym. stretch	2221	4.84E − 17	1605	1.44E − 17
ν_9	e	CH_3 deformation	1469	1.48E − 18	1468	9.51E − 19
ν_{10}	e	SiH_3 deformation	965	1.58E − 17	692	4.65E − 18
ν_{11}	e	CH_3, SiH_3 rocking	896	2.26E − 17	851	6.77E − 18
ν_{12}	e	CH_3, SiH_3 rocking	525	3.80E − 18	416	1.45E − 18
			Staggered CH_3SiH_2		Staggered CH_3SiD_2	
ν_1	a′	CH_3 asym. stretch	3091	1.16E − 18	3091	1.15E − 18
ν_2	a′	CH_3 sym. stretch	3021	1.15E − 18	3021	1.16E − 18
ν_3	a′	SiH_2 sym. stretch	2178	1.45E − 17	1558	8.57E − 18
ν_4	a′	CH_3 deformation	1463	9.78E − 19	1463	1.02E − 18
ν_5	a′	CH_3 umbrella	1291	1.27E − 18	1291	9.08E − 19
ν_6	a′	SiH_2 bending	938	1.66E − 17	708	9.86E − 18
ν_7	a′	CH_3, SiH_2 rocking	851	1.31E − 17	811	8.74E − 18
ν_8	a′	C–Si stretch	681	2.85E − 18	643	1.61E − 18
ν_9	a′	CH_3, SiH_2 rocking	570	2.54E − 18	450	2.60E − 18
ν_{10}	a″	CH_3 asym. stretch	3112	1.32E − 18	3112	1.27E − 18
ν_{11}	a″	SiH_2 asym stretch	2203	2.60E − 17	1594	1.44E − 17
ν_{12}	a″	CH_3 deformation	1458	1.23E − 18	1458	1.40E − 18
ν_{13}	a″	CH_3, SiH_2 deformation	895	7.23E − 18	851	4.82E − 18
ν_{14}	a″	CH_3, SiH_2 deformation	530	8.87E − 19	413	7.62E − 19
ν_{15}	a″	Torsion	177	5.55E − 20	155	2.71E − 20
			Staggered CH_2SiH_3		Staggered CH_2SiD_3	
ν_1	a′	CH_2 sym. stretch	3122	7.69E − 19	3122	7.79E − 19
ν_2	a′	SiH_3 sym. stretch	2221	1.24E − 17	1568	8.02E − 18
ν_3	a′	SiH_3 asym. stretch	2185	1.89E − 17	1591	1.12E − 17
ν_4	a′	CH_2 bending	1405	3.66E − 19	1404	1.52E − 19
ν_5	a′	SiH_3 umbrella	951	3.56E − 17	768	1.53E − 17
ν_6	a′	SiH_3 deformation	948	1.05E − 17	682	6.69E − 18
ν_7	a′	C–Si stretching	748	2.19E − 18	672	7.70E − 18
ν_8	a′	SiH_3 rocking	666	1.65E − 17	606	1.30E − 17
ν_9	a′	CH_2 umbrella	525	1.01E − 18	436	2.25E − 19
ν_{10}	a″	CH_2 asym. stretch	3214	5.86E − 19	3214	5.58E − 19
ν_{11}	a″	SiH_3 asym. stretch	2224	2.22E − 17	1607	1.33E − 17
ν_{12}	a″	SiH_3 deformation	961	7.27E − 18	689	3.97E − 18
ν_{13}	a″	CH_2, SiH_3 rocking	847	1.03E − 17	795	6.18E − 18
ν_{14}	a″	CH_2, SiH_3 rocking	526	1.58E − 18	423	1.45E − 18
ν_{15}	a″	Torsion	17	4.98E − 22	15	8.97E − 22

(331) kJ mol^{-1}, whereas the fragmentation of the silicon–hydrogen and carbon–hydrogen bonds to form the methylsilyl radical $CH_3SiH_2(X^2A')$ plus a hydrogen atom and the silylmethyl $CH_2SiH_3(X^2A')$ plus atomic hydrogen from methylsilane requires 375 (367) kJ mol^{-1} and 414 (404) kJ mol^{-1}, respectively. The overall energetics to form silylmethyl $CH_2SiH_3(X^2A')$ and methylsilyl radical $CH_3SiH_2(X^2A')$ via Eq. (9) was calculated to be +859 and +820 kJ mol^{-1}. These values agree very well with those derived from enthalpies of formation as listed in [21,22] and in the NIST database [67].

$$CH_4(X^1A_1) + SiH_4(X^1A_1) \rightarrow H_2SiCH_3/H_3SiCH_2(X^2A') + 3H(^2S_{1/2}). \quad (9)$$

Tables 2 and 3 summarize the vibrational frequencies and infrared intensities of $CSiH_6$ and $CSiH_5$ systems calculated with the B3LYP/6-311G(d,p) level of theory. Table 2 includes the frequencies and intensities of partially deuterated species of methylsilane, silylmethyl, and methylsilyl at their energy minima. Table 3 shows the frequencies located at the transition states which have one imaginary vibrational mode for each species.

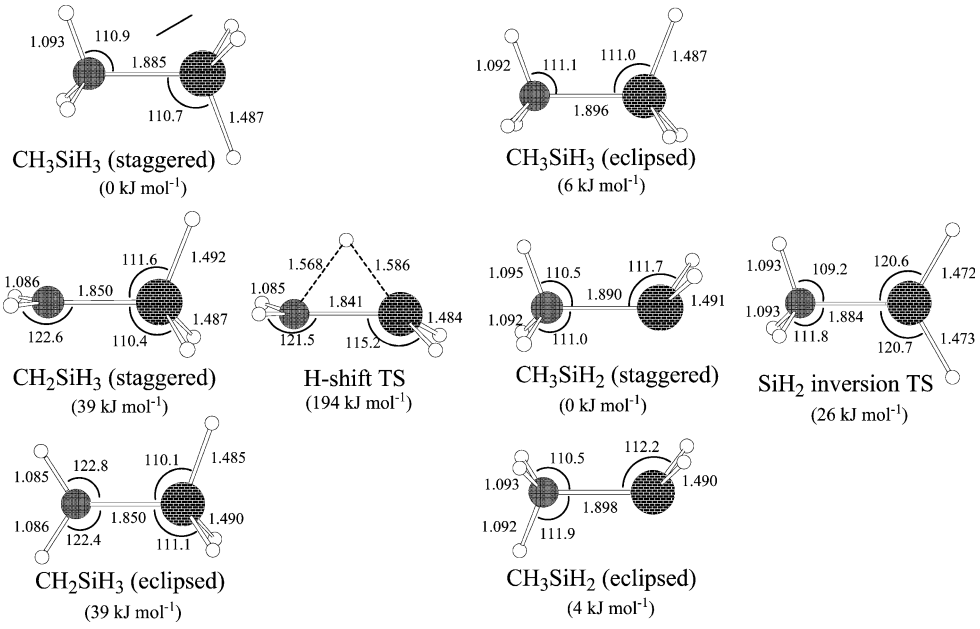

Fig. 2. Optimized structures of methylsilane (CH_3SiH_3) (staggered and eclipsed; top row) as well as the methylsilyl $CH_3SiH_2(X^2A')$ and silylmethyl $CH_2SiH_3(X^2A')$ radicals together with the transition state involved in the hydrogen migration and the SiH_2 inversion of CH_3SiH_2 (middle row) calculated with B3LYP/6-311G(d,p) level of theory. The eclipsed conformers of the methylsilyl and silylmethyl radicals are also shown (bottom row). The bond lengths and bond angles are in Angstrom and degrees, respectively. The values in parentheses are the relative energies calculated with the CCSD(T) method.

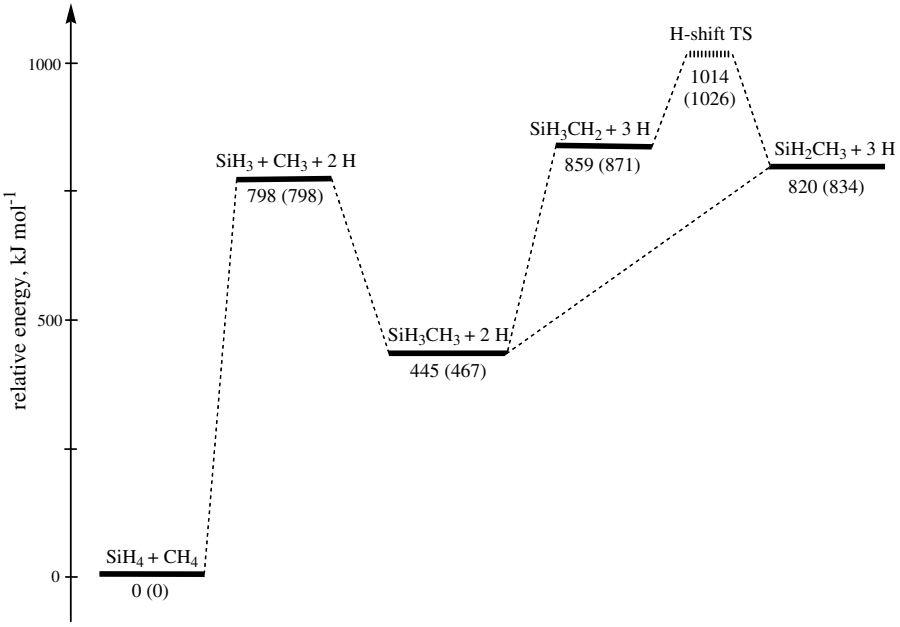

Fig. 3. Schematic potential energy surface of the reaction of methane with silane to form the methylsilyl radical $CH_3SiH_2(X^2A')$ and the silylmethyl $CH_2SiH_3(X^2A')$ radical. Energies have been obtained with the CCSD(T) method; zero point vibrational energies are included. The transition state involved in the hydrogen migration is denoted as a bold, dashed line. The values in parentheses are the relative energies obtained with the B3LYP level of theory.

5. Experimental results

Upon irradiation of the silane–methane sample, prominent absorptions of the silyl radical, $SiH_3(X^2A_1)$, and of the methyl radical, $CH_3(X^2A_2'')$, developed instantaneously at 722 and 609 cm^{-1}, respectively (Table 4). The positions of both ν_2 umbrella modes correlate nicely previous studies utilizing hydrogen, neon, argon, and krypton (721–738 cm^{-1}; silyl) [68–70] as well as neon, argon, and nitrogen matrices (603–611 cm^{-1}; methyl)

Table 3
Unscaled vibrational frequencies (cm^{-1}) and infrared intensities (cm $molecule^{-1}$) of the eclipsed conformers of CH_3SiH_3, CH_3SiH_2, and CH_2SiH_3 calculated with B3LYP/6-311G(d,p) level of theory

		Characterization	Frequency	Intensity
Eclipsed CH_3SiH_3				
ν_1	a	CH_3 sym. stretch	3040	1.19E − 18
ν_2	a	SiH_3 sym. stretch	2220	1.19E − 17
ν_3	a	CH_3 umbrella	1309	2.54E − 18
ν_4	a	SiH_3 umbrella	957	3.87E − 17
ν_5	a	C–Si stretching	687	2.68E − 18
ν_6	a	Torsion	190*i*	0.00E + 00
ν_7	e	CH_3 asym. stretch	3111	3.16E − 18
ν_8	e	SiH_3 asym. stretch	2219	4.74E − 17
ν_9	e	CH_3 deformation	1475	1.32E − 18
ν_{10}	e	SiH_3 deformation	965	1.69E − 17
ν_{11}	e	CH_3, SiH_3 rocking	875	1.76E − 17
ν_{12}	e	SiH_3,CH_3 rocking	575	5.99E − 18
Transition state between CH_3SiH_2 and CH_2SiH_3				
ν_1	a′	CH_2 sym. stretch	3129	5.68E − 20
ν_2	a′	SiH_2 sym. stretch	2199	1.39E − 17
ν_3	a′	Si···H stretch	1877	1.96E − 18
ν_4	a′	CH_2 scissor	1375	1.13E − 18
ν_5	a′	SiH_2 scissor	897	1.62E − 17
ν_6	a′	C–Si stretch	776	2.47E − 18
ν_7	a′	CH_2, SiH_2 wagging	668	1.41E − 18
ν_8	a′	CH_2, SiH_2 wagging	603	1.33E − 17
ν_9	a″	H shift	1725*i*	9.35E − 17
ν_{10}	a″	CH_2 asym. stretch	3231	3.32E − 19
ν_{11}	a″	SiH_2 asym. stretch	2238	2.17E − 17
ν_{12}	a″	H rolling	1003	3.21E − 18
ν_{13}	a″	CH_2, SiH_2 rock	828	7.34E − 18
ν_{14}	a″	CH_2, SiH_2 rock	532	6.60E − 19
ν_{15}	a″	CH_2, SiH_2 twist	265	9.50E − 21
Eclipsed CH_3SiH_2				
ν_1	a′	CH_3 asym. stretch	3102	1.06E − 18
ν_2	a′	CH_3 sym. stretch	3032	1.22E − 18
ν_3	a′	SiH_2 sym. stretch	2180	1.44E − 17
ν_4	a′	CH_3 deformation	1459	1.06E − 18
ν_5	a′	CH_3 umbrella	1294	1.19E − 18
ν_6	a′	SiH_2 scissor	941	1.58E − 17
ν_7	a′	CH_3, SiH_2 rock	834	8.94E − 18
ν_8	a′	C–Si stretch	677	3.30E − 18
ν_9	a′	SiH_2 umbrella	610	4.39E − 18
ν_{10}	a″	CH_3 asym. stretch	3109	1.17E − 18
ν_{11}	a″	SiH_2 asym. stretch	2205	2.52E − 17
ν_{12}	a″	CH_3 deformation	1472	7.53E − 19
ν_{13}	a″	CH_3, SiH_2 rocking	854	6.32E − 18
ν_{14}	a″	SiH_2,CH_3 rocking	569	1.42E − 18
ν_{15}	a″	Torsion	174*i*	3.32E − 22
Eclipsed CH_2SiH_3				
ν_1	a′	CH_2 asym. stretch	3214	5.67E − 19
ν_2	a′	CH_2 sym. stretch	3122	7.80E − 19
ν_3	a′	SiH stretch	2231	1.84E − 17
ν_4	a′	SiH_2 sym. stretch	2205	1.31E − 17
ν_5	a′	CH_2 scissor	1405	3.68E − 19
ν_6	a′	SiH_3 deformation	961	7.40E − 18
ν_7	a′	SiH_3 umbrella	951	3.71E − 17
ν_8	a′	CH_2 rocking	847	1.04E − 17
ν_9	a′	C–Si stretch	748	2.17E − 18
ν_{10}	a′	CH_2, SiH_3 rocking	527	1.61E − 18
ν_{11}	a″	SiH_2 asym. stretch	2195	2.21E − 17
ν_{12}	a″	SiH_3 deformation	947	8.90E − 18
ν_{13}	a″	CH_2 inversion, SiH_3 rocking	663	1.64E − 17
ν_{14}	a″	CH_2 inversion, SiH_3 rocking	526	9.10E − 19
ν_{15}	a″	Torsion	61*i*	7.37E − 20

The frequencies of the transition state connecting the methylsilyl and the silylmethyl radicals are also included.

Table 4
Compilation of newly observed species and their absorptions in low temperature silane–methane matrices

Frequency (cm^{-1})	Fundamental	Carrier
609	ν_2	CH_3
722	ν_2	SiH_3
826	ν_{12}	C_2H_6
1380	ν_{16}	C_2H_6
1462	ν_{11}	C_2H_6
2880	ν_5	C_2H_6
2973	ν_{10}	C_2H_6
826	ν_6	Si_2H_6
934	ν_{11}	Si_2H_6
2142	$\nu_{5/4}$	Si_2H_6
691	ν_5	CH_3SiH_3
863	ν_{11}	CH_3SiH_3
946	ν_{10}	CH_3SiH_3
976	ν_4	CH_3SiH_3
1254	ν_3	CH_3SiH_3
2142	ν_2	CH_3SiH_3
530	ν_9	C_2H_5
2848	ν_3	C_2H_5
2939	ν_2	C_2H_5
852	ν_6	Si_2H_5
654	ν_8	CH_3SiH_2
1414	ν_{12}	CH_3SiH_2
1251	ν_5	CH_3SiH_2
645	ν_8	CH_2SiH_3

[71]. Note that the umbrella mode holds the highest absorption coefficient (1.4×10^{-17} cm); the remaining fundamentals ($\nu_1(a_1')$ (infrared inactive)), $\nu_3(e')$ (1.2×10^{-18} cm), and $\nu_4(e')$ (6.6×10^{-19} cm) of the methyl radical cannot be observed. The ν_4 deformation (925–928 cm^{-1}; 2.2×10^{-17} cm) [68–70] and the ν_3 silicon–hydrogen stretching mode (2185 cm^{-1}; 4.3×10^{-17} cm) [72] remain unobservable in our experiments because they are obscured by the fundamentals of the silane ice; the infrared intensity of the ν_1 mode (8.3×10^{-19} cm) is too weak to be observed. Also, absorptions at 826, 1380, 1462, 2880, and 2973 cm^{-1} showed up immediately at the beginning of the irradiation. These features were assigned to the ν_{12}, ν_6, ν_{11}, ν_5, and ν_{10} modes of the ethane (C_2H_6) molecule; the remaining fundamentals of ethane are infrared inactive. Similarly, we detected the absorptions of the disilane species (Si_2H_6) at 826 cm^{-1} (ν_6, shoulder), 934 cm^{-1} (ν_{11}), and 2142 cm^{-1} ($\nu_{5/10}$, shoulder). The detection of the MH_3 and M_2H_6 species (M = C, Si) is in perfect agreement with the electron exposure experiments of the neat silane [55] and methane ices [54]. Here, the ethane and disilane molecule were simply the recombination products of two methyl and silyl radicals, respectively (Eqs. (2) and (5)). The spectra of these species have been reported previously [54,55] and are not shown here.

Since ethane and silane could be detected, we would also expect the formation of the methylsilane molecule (CH_3SiH_3) via cross recombination of a methyl with the silyl radical through Eq. (7). Indeed, we were able to observe new bands appearing instantaneously with the start of the irradiation at 691, 863, 946, 976, 1254, 2142 cm^{-1} (Table 4). Two absorptions are shown in Fig. 4. These positions can be assigned to the $\nu_5(a_1$, C–Si stretching), ν_{11}(e, CH_3 rocking), $\nu_4(a_1$, SiH_3 symmetric deformation), ν_{10}(e, SiH_3 asymmetric deformation), $\nu_3(a_1$, CH_3 symmetric deformation), and $\nu_2(a_1$, CH_3 symmetric stretch) fundamentals of the methylsilane molecule; note that the 2142 cm^{-1} peak is actually composed of two absorptions from methylsilane and from ethane. These data agree very well with our computational studies (Table 2) after scaling by 0.97 – a reasonable value for the B3LYP method – and also with previous experiments [28].

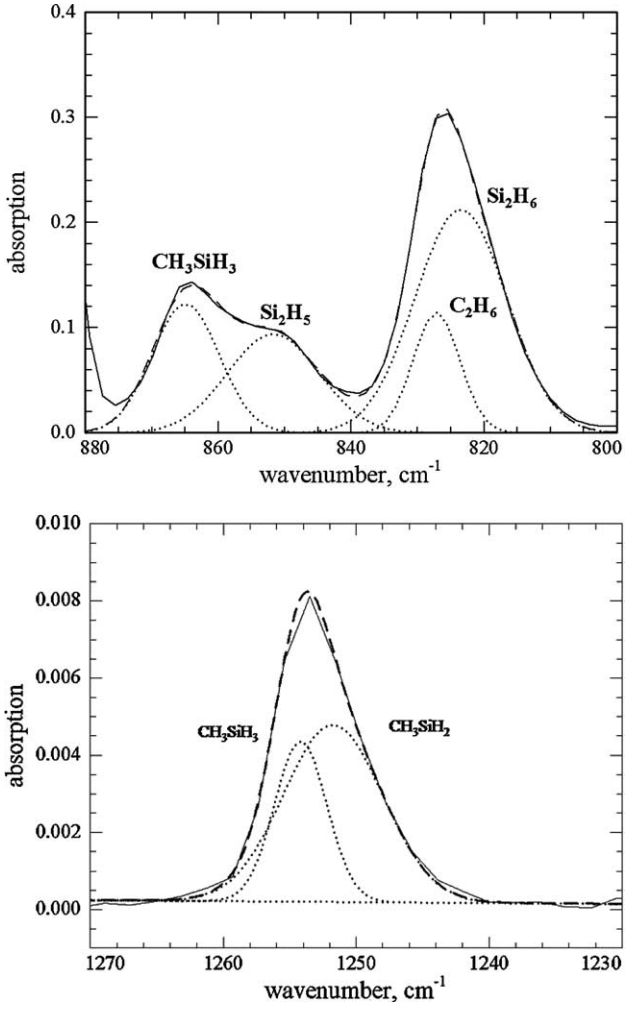

Fig. 4. Top: The absorption feature of the methylsilane molecule at 863 cm^{-1} (ν_{11}). The ν_6 mode of the disilyl radical, the ν_{12} absorption of ethane and the ν_6 fundamental of disilane (revealed by deconvolution) are also shown. Bottom: Deconvoluted peak consisting of the 1254 cm^{-1} absorption of the methylsilane molecule (ν_3) and the 1250 cm^{-1} feature of the methylsilyl radical (ν_5). Both spectra were taken after 60 min irradiation time.

We could identify also bands at 530, 2848, and 2939 cm^{-1} (Table 4); these features agree very well with the CH_2 out of plane (ν_9, a′), CH_3 stretch (ν_3, a′), and CH_3 symmetric stretch (ν_2, a′) positions of the ethyl radical (C_2H_5) reported previously [73]. Also, these three peaks have the highest infrared absorption coefficients of 8.3×10^{-18} cm, 5.3×10^{-18} cm, and 4.6×10^{-18} cm of the fundamentals of the ethyl radical. Similarly, we were able to observe the disilyl radical (Si_2H_5) via its strongest absorption of the umbrella mode at 852 cm^{-1}(ν_6, a′, 6.9×10^{-17} cm) [55]. Compared to a previous observation in a silane matrix, this position is blue shifted by 9 cm^{-1}. Note that the less intense absorptions at about 945 and 2140 cm^{-1} overlap with the intensive modes of the methylsilane molecule.

Recall that both the ethyl and disilyl radicals were found to be formal decomposition products of the corresponding closed shell ethane and disilane molecules (Eqs. (3) and (6)). Therefore, we could predict that either the CH_3SiH_2 and/or the CH_2SiH_3 radical should be formed via fragmentation of the methylsilane molecule, too. Indeed, we were able to monitor three fundamentals of the methylsilyl radical $CH_3SiH_2(X^2A')$ at 654 cm^{-1} (ν_8), 1414 cm^{-1}(ν_{12}), and 1251 cm^{-1}(ν_5; shoulder) as shown in Table 4. These observed frequencies are in very good agreement with our calculations (Table 2) predicting – after scaling by a factor of 0.97 – peak positions at 660, 1414, and 1252 cm^{-1}. Most importantly, the intensity ratio of the ν_8 versus ν_{12} fundamentals of (2.7 ± 0.1):1 correlate very well with the theoretically predicted one of (2.3 ± 0.5):1. The peak at 1414 cm^{-1} (ν_{12}) is weaker. As the irradiation time increases, a shoulder developed at the low frequency site of the ν_8 absorption; a deconvolution routine utilizing Gaussian peak profiles yielded a second peak at 645 cm^{-1} (Fig. 5). This could be assigned to the ν_8 of the silylmethyl radical $CH_2SiH_3(X^2A')$; theory predicts – after scaling by 0.97–646 cm^{-1}. Accounting for the absorption coefficients of the 660 and the 645 cm^{-1} fundamentals, we derived a ratio of the methylsilyl versus silylmethyl radical concentration at the end of the irradiation of (22 ± 3):1, i.e., a preferential formation of the thermodynamically more stable isomer.

To confirm these assignments, we prepared d4-silane–methane ices (SiD_4–CH_4) and subjected this mixture also to a 5 keV electron irradiation – hoping to synthesize partially deuterated $CH_3SiD_2(X^2A')$ and/or $CH_2SiD_3(X^2A')$ radicals. As expected, we observed besides the methyl and ethyl radicals, the perdeuterated silyl radical via its ν_2 absorption at 541 cm^{-1} (Table 5). Also, prominent peaks are visible at 606 and 1541 cm^{-1}, which could be attributed to the perdeuterated disilane molecule; a prominent absorption also emerges at 625 cm^{-1} (perdeutero disilyl radical). These positions are in excellent agreement with previous irradiation exposures of pure d4-silane samples at 10 K [55].

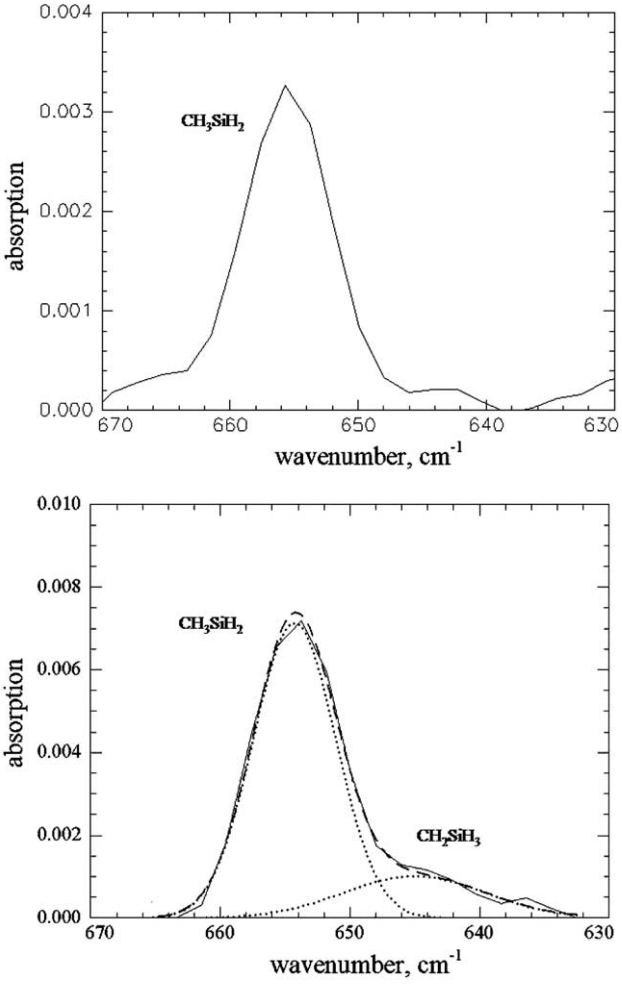

Fig. 5. Top: Absorption of the methylsilyl radical, $CH_3SiH_2(X^2A')$, at 654 cm^{-1} (ν_8) after 10 min irradiation time. Bottom: Deconvoluted absorptions of the methylsilyl radical, $CH_3SiH_2(X^2A')$, at 654 cm^{-1} (ν_8) and of the silylmethyl radical, $CH_2SiH_3(X^2A')$, at 645 cm^{-1} (ν_8) after 60 min irradiation time.

Most importantly, we were also able to assign six fundamentals of the d3-methylsilane molecule (CH_3SiD_3) (Table 5) – a potential precursor to form the d2-methylsilyl radical and/or the d3-silylmethyl species at 10 K. It is also worth mentioning that we see additional features at 1167 and 684 cm^{-1}. Comparing these absorptions with literature values of partially deuterated methane and silane molecules [74] suggests that these peaks can be attributed to the ν_4 fundamentals of the CH_3D and SiD_3H molecules, respectively. The identification of these species is important evidence that upon electron exposure of the d4-silane and methane molecules, the latter undergo initially carbon–hydrogen and silicon-deuterium bond rupture processes to form the spectroscopically observed methyl and d3-silyl radicals; the deuterium and hydrogen atoms are mobile at 10 K and can also cross recombine with the methyl radical and the d3-silyl radical to synthesize CH_3D and SiD_3H molecules, respectively, via Eqs. (10) and (11):

Table 5
Compilation of newly observed species and their absorptions in low temperature d4-silane–methane matrices

Frequency (cm^{-1})	Fundamental	Carrier
1167	ν_4	CH_3D
684	ν_4	SiD_3H
541	ν_2	SiD_3
606	ν_6	Si_2D_6
1541	ν_5	Si_2D_6
640	ν_5	CH_3SiD_3
735	ν_4	CH_3SiD_3
1253	ν_3	CH_3SiD_3
1410	ν_9	CH_3SiD_3
1583	ν_8	CH_3SiD_3
2923	ν_1	CH_3SiD_3
625	ν_6	Si_2D_5
781	ν_7	CH_3SiD_2
1415	ν_{12}	CH_3SiD_2
1419	ν_4	CH_3SiD_2
1546	ν_{11}	CH_3SiD_2
582	ν_8	CH_2SiD_3
749	ν_5	CH_2SiD_3
771	ν_{13}	CH_2SiD_3

The absorptions of the methyl radical, ethane, and the ethyl radical are shifted by up to 3 cm^{-1} compared to the silane–methane matrix (Table 4) and are not reported here.

$$CH_3(X^2A_2'') + D(^2S_{1/2}) \rightarrow CH_3D(X^1A_1) \quad (10)$$

$$SiD_3(X^2A_1) + H(^2S_{1/2}) \rightarrow SiD_3H(X^1A_1). \quad (11)$$

Most importantly, we were also able to observe four fundamentals of the doubly deuterated methylsilyl radical (CH_3SiD_2) at 781, 1415, 1419, and 1546 cm^{-1}(Table 5). These data are in excellent agreement with our calculated frequencies predicting – after scaling by 0.97 – absorptions at 786, 1414, 1419, and 1546 cm^{-1} (Table 2). Likewise, the second isomer, the d3-silylmethyl radical, could be also confirmed experimentally via its bands at 582, 749, and 771 cm^{-1}. Here, these values also agree very well with the computed frequencies (588, 745, 771 cm^{-1}) (Tables 2 and 5).

6. Discussion and summary

Our results suggest that the response of the silane–methane target upon electron irradiation is shaped initially by silicon–hydrogen and carbon–hydrogen bond rupture processes in the silane and methane molecules, respectively. This leads to the synthesis of the silyl radical, $SiH_3(X^2A_1)$, and the methyl radical, $CH_3(X_2A_2'')$, plus atomic hydrogen via Eqs. (1) and (4). However, each hydrogen atom demands an excess energy – the lattice binding energy – of a few tens of kJ mol^{-1} to escape from the initially formed [$SiH_3\cdots H$] and matrix cages [$CH_3\cdots H$] [75]. If this energy cannot be supplied, the hydrogen atom will react back with the silyl and methyl radicals to 'recycle' silane and methane. The presence of mobile hydrogen atoms during the irradiation is supported by two findings. First, the detection of singly hydrogenated silane, $SiD_3H(X^1A_1)$, and singly deuterated methane, $CH_3D(X^1A_1)$, during the exposure of d4-silane–methane targets to electrons strongly indicates the reaction of mobile hydrogen atoms with d3-silyl and of mobile deuterium atoms with methyl radicals according to Eqs. (10) and (11), respectively. Second, our mass spectrometric data also verify the formation of mobile hydrogen atoms in the ice at 10 K (Fig. 6). The ion current of $m/e = 2$ (H_2) increase sharply as the electron beam is switched on and reaches quickly a plateau. As the irradiation is stopped after 60 min, the $m/e = 2$ signal decreases quickly. Since we were unable to identify any SiH_x or CH_x species in the solid state except the silyl and methyl radicals, we can conclude that the molecular hydrogen is formed via recombination of two hydrogen atoms in the ice. It should be stressed that $m/e = 2$ present the only signal detected with the mass spectrometer during the irradiation of the ices. This indicates that the molecular hydrogen in the gas phase does not represent a fragment from any hydrogenated silicon and/or carbon bearing molecules. Note that similar to pure silane experiments, the mass spectrometric data also show that after the irradiation, the matrix stores thermalized hydrogen atoms; these atoms diffuse upon warming the matrix (here at 14 K) and recombine to molecular hydrogen. The latter is being released into the gas phase (Fig. 6).

How can our data explain the formation of the methylsilane and the hitherto elusive silylmethyl and methylsilyl radicals? Recall that each electron can release its kinetic energy via multiple energy transfers to various silane and methane molecules. Utilizing the CASINO code [76], we find that each 5 keV electron loses 0.7 ± 0.1 keV of its kinetic energy while penetrating

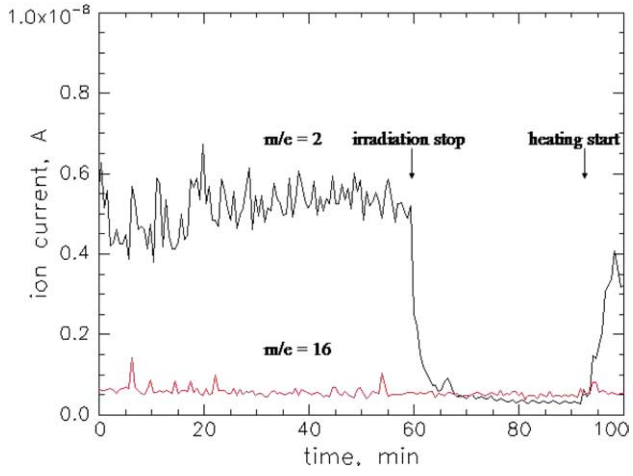

Fig. 6. Temporal profile of the methane ($m/e = 16$; bottom) and molecular hydrogen ($m/e = 2$; bottom) evolution during the irradiation (60 min), the isothermal phase at 10 K (30 min), and the heating of the silane–methane sample.

the methane–silane target; this corresponds to an averaged electronic energy transfer of 3.3 ± 0.5 keV μm^{-1}. Also, since the dissociation energy of the Si–H and C–H bonds are 376 kJ mol^{-1} (3.9 eV) and 439 kJ mol^{-1} (4.5 eV) [77,78], each electron can form up to 180 silyl and 155 methyl radicals in the matrix. Considering the composition of the matrix, 100 silyl and about 70 methyl radicals should be generated statistically per implanted electron. Due to the immobility of silyl and methyl radicals at 10 K, only *neighboring* radicals can recombine to form disilane, ethane, and methylsilane inside the trajectory at 10 K. Note that the formed methylsilane molecule is initially vibrationally excited. This internal energy can be either diverted via phonon coupling to the matrix thus stabilizing the methylsilane molecule (as detected via infrared spectroscopy), fragments back to the silyl and methyl radical, or loses a hydrogen atom thus releasing the excess energy predominantly as kinetic energy of the hydrogen atom. In this case, the vibrationally excited methylsilane molecule should undergo either a Si–H or C–H bond cleavage to form the methylsilyl and the silylmethyl radical. Based on our experiments, we only detect the methylsilyl radical with the onset of the electron irradiation. This suggests a preferential rupture of the Si–H bond in the vibrationally excited methylsilane species; this correlates nicely with inherent bond strengths (Fig. 3) and also with ^{60}Co γ irradiation of methylsilane yielding solely the energetically preferred CH_3SiH_2 radical [38,39]. Here, the Si–H bond is 39 kJ mol^{-1} weaker than the C–H bond – making it easier to dissociate to the methylsilyl than to the silylmethyl radical. However, as the irradiation time increases, we see additional features of the silylmethyl radical. This could be explained by a radiolysis of the methylsilane molecule, i.e., a decomposition of the methylsilane molecule upon energy transfer by the energetic electron followed by decomposition to methylsilyl and silylmethyl. Our scenario postulates that at the end of the irradiation, we should have formed an excess of methylsilyl compared to silylmethyl radicals; this has been confirmed experimentally by observing a methylsilyl versus silylmethyl ratio of 22 ± 3. For completeness, we would like to address briefly the possibility of silicon and carbon atoms reacting with methane and silane molecules. Maier et al. [41] observed that at 10 K, silicon atoms did not react with methane via insertion due to an inherent entrance barrier. Likewise, the reaction of ground state carbon atoms is prohibited since an entrance barrier blocks this pathway [19]. Most important, these reactions would lead to $SiCH_4$ isomers which were clearly not observed in our experiment. Note that a reaction of free silicon and carbon atoms with mobile hydrogen atoms in our matrix is also expected to form simple silicon hydrides such as SiH and SiH_2 as well as CH and CH_2 through barrier-less recombination reactions, which in turn could react with methane and silane via insertion processes. However, we would like to recall that this represents a time-delayed multi-step reaction mechanism which could not account for the prompt observation of methylsilane upon onset of the irradiation. Finally, we were unable to observe the well-known infrared features of SiH, SiH_2, CH, and CH_2 [67]; these considerations suggest that the reactions of small carbon and silicon hydrogenated molecules can be likely ruled out.

Summarized, we presented the very first infrared spectroscopic detection of two hitherto elusive $SiCH_5$ species, i.e., the methylsilyl $CH_3SiH_2(X^2A')$ and silylmethyl $CH_2SiH_3(X^2A')$ radicals, together with their partially deuterated counterparts. Since both the methane and silane precursors are present in the circumstellar envelope of the carbon star IRC+10216, the ν_8, ν_{12}, and ν_5 (CH_3SiH_2) as well as ν_8 (CH_2SiH_3) fundamentals can now be utilized to search for these species in the circumstellar shell with powerful infrared telescopes. Note that the computed dipole moments of 0.739 Debye (CH_3SiH_3; $A = 56.119$ GHz, $B = C = 10.821$ GHz), 0.806 Debye (CH_3SiH_2, $A = 73.007$ GHz, $B = 11.583$ GHz, $C = 11.027$ GHz), and 0.650 Debye (CH_2SiH_3, $A = 67.012$ GHz, $B = 11.952$ GHz, $C = 11.475$ GHz) suggest that an infrared spectroscopic detection of these species is actually more likely than an identification via radio telescopes. In addition, the presented infrared frequencies help to follow the time-dependent concentration profiles of crucial organo-silane species – here both the methylsilyl and the silylmethyl radicals – in real time in chemical vapor deposition to ultimately optimize these processes.

Acknowledgments

The experiments were supported by the University of Hawai'i at Manoa (DS, CJB, RIK). The computations were carried out at the computer center of the Institute for Molecular Science, Japan, and supported by the Grants-in-Aid for Scientific Research on Priority Areas from the Ministry of Education, Science, and Culture, Japan (Y.O.).

References

[1] K.S. Nahm et al., J. Chem. Eng. Japan 34 (2001) 692.
[2] L.V. Interrante, B. Han, J.B. Hudson, C. Whitmarsh, Appl. Surf. Sci. 46 (1990) 5.
[3] M. Shinohara, Y. Kimura, D. Shoji, M. Niwano, Appl. Surf. Sci. 175/176 (2001) 591.
[4] S. Nishino, Y. Hazuki, H. Matsunami, T. Tanaka, J. Electrochem. Soc. 127 (1980) 2674.
[5] K. Shibahara, S. Nishino, H. Matsunami, J. Cryst. Growth 78 (1986) 538.
[6] R. Fantoni, F. Bjnen, N. Djuric, S. Piccirillo, Appl. Phys. B 52 (1991) 176.
[7] M. Foster, B. Darlington, J. Scharff, A. Campion, Surf. Sci. 375 (1997) 35.

[8] L.A. Okada, A.C. Dillon, A.W. Ott, S.M. George, Surf. Sci. 418 (1998) 353.
[9] S.L. Girshickm, M.T. Swihart, S.M. Hu, M.R. Mahajan, S. Nijhawan, Proc. Electrochem. Soc. 98 (1999) 215.
[10] M.T. Swihart, S.L. Girshick, J. Phys. Chem. B 103 (1999) 64.
[11] P. Ho, M.E. Coltrin, J.S. Binkley, C.F. Melius, J. Phys. Chem. 90 (1986) 3399.
[12] M.C. Ernst, A.F. Sax, J. Kalcher, Chem. Phys. Lett. 216 (1993) 189.
[13] M.T. Swihart, J. Phys. Chem. A 104 (2000) 6083.
[14] C. Pak, J.C. Rienstra-Kiracofe, H.F. Schaefer, J. Phys. Chem. A 104 (2000) 11232.
[15] S. Hundsicker, R.O. Jones, J. Chem. Phys. 105 (1996) 5048.
[16] M. Pellarin et al., Chem. Phys. Lett. 277 (1997) 96.
[17] Z.Y. Jian et al., Chem. Phys. 290 (2003) 223.
[18] B.E. Turner, ApJ 376 (1991) 573.
[19] R.I. Kaiser, Chem. Rev. 102 (2002) 1309.
[20] D.M. Goldhaber, A.L. Betz, ApJ 279 (1984) L55.
[21] M.D. Allendorf, C.F. Melius, J. Phys. Chem 96 (1992) 428.
[22] C.G. Pitt, J. Organomet. Chem. 61 (1973) 49.
[23] J.L. Duncan, A.M. Ferguson, Spectrosc. Chim. Acta A 52 (1996) 1515.
[24] J.L. Duncan, J.L. Harvie, D.C. McKean, S. Cradock, J. Mol. Struct. 145 (1986) 225.
[25] D.C. McKean, I. Torto, J.E. Boggs, K. Fan, J. Mol. Struct. (THEOCHEM) 260 (1992) 27.
[26] J.L. Duncan, A.M. Ferguson, D.C. McKean, J. Mol. Spectrosc. 168 (1994) 522.
[27] N. Moazzen-Ahmadi, I. Ozier, E.H. Wishnow, H.P. Gush, J. Mol. Spectrosc. 170 (1995) 516.
[28] R.E. Wilde, J. Mol. Spectrosc. 8 (1962) 427.
[29] M. Randic, Spectrochim. Acta 18 (1962) 115.
[30] J.S. Francisco, H.B. Schlegel, J. Chem. Phys. 88 (1988) 3736.
[31] M.A. Ring, H.E. O'Neal, S.F. Rickborn, B.A. Sawrey, Organometallics 2 (1983) 1891.
[32] Z.X. Wang, M.B. Huang, J. Chem. Soc., Faraday Trans. 94 (1998) 635.
[33] N.L. Arthur, P. Potzinger, B. Heimann, H.P. Steenbergen, J. Chem. Soc., Faraday Trans. 85 (1989) 1447.
[34] Q.Z. Zhang et al., Chin. Chem. Lett. 11 (2000) 119.
[35] R. Damrauer, A.J. Crowell, C.F. Craig, J. Am. Chem. Soc 125 (2003) 10759.
[36] S.K. Shin, J.L. Beauchamp, J. Am. Chem. Soc 111 (1989) 900.
[37] K. Komaguchi, Y. Ishiguri, H. Tachikawa, M. Shiotani, Phys. Chem. Chem. Phys. 4 (2002) 5276.
[38] J.H. Sharp, M.C.R. Symons, J. Chem. Soc. A (1970) 3084.
[39] S.W. Bennett, C. Eaborn, A. Hudson, R.A. Jackson, K.D.J. Root, J. Chem. Soc. A (1970) 348.
[40] V.N. Khabashesku, K.N. Kudin, J.L. Margrave, J. Mol. Struct. 443 (1998) 175.
[41] G. Maier, H.P. Reisenauer, J. Glatthaar, Chem. Eur. J. 8 (2002) 4383.
[42] S. Bailleux et al., J. Chem. Phys. 106 (1997) 10016.
[43] H.J. Koehler, H. Lischka, J. Am. Chem. Soc. 104 (1982) 5884.
[44] A.E. Ketvirtis, D.K. Bohme, A.C. Hopkinson, J. Phys. Chem. 99 (1995) 16121.
[45] A.A. Bengali, D.G. Leopold, J. Am. Chem. Soc. 114 (1992) 9192.
[46] T.C. Smith, H. Li, D.J. Clouthier, J. Chem. Phys. 114 (2001) 9012.
[47] R.K. Hilliard, R.S. Grev, J. Chem. Phys. 107 (1997) 8823.
[48] R. Stegemann, G. Frenking, J. Comput. Chem. 17 (1996) 781.
[49] R. Cereasa, D. Cossart, M. Vervloet, J.M. Robbe, J. Chem. Phys. 112 (2000) 10806.
[50] J.M. Robbe, H. lavendy, J.P. Flament, G. Chambaud, Chem. Phys. Lett. 267 (1997) 91.
[51] D.S. Han, C.M.L. Rittby, W.R.M. Graham, J. Chem. Phys. 108 (1998) 3504.
[52] T.C. Smith, H. Li, D.J. Clouthier, J. Am. Chem. Soc. 121 (1999) 6068.
[53] L. Sari, J.M. Gonzales, Y. Yamaguchi, H.F. Schaefer, J. Chem. Phys. 114 (2001) 4472.
[54] C. Bennett, R.I. Kaiser, ApJ (submitted).
[55] D. Sillars, C.J. Bennett, Y. Osamura, R.I. Kaiser, Chem. Phys. 305 (2004) 141.
[56] C. Bennett, A.M. Mebel, R.I. Kaiser, Phys. Chem. Chem. Phys. 6 (2004) 735.
[57] W.M. Sears, J.A. Morrison, J. Chem. Phys. 62 (1975) 2736.
[58] G. Baciocco, P. Calvani, S. Cunsolo, Int. J. Infrared Millimeter Waves 8 (1987) 923.
[59] W.M. Sears, J.A. Morrison, J. Chem. Phys. 62 (1975) 2736.
[60] A.D. Becke, J. Chem. Phys. 98 (1993) 5648.
[61] G.D. Purvis, R.J. Bartlett, J. Chem. Phys. 76 (1982) 1910.
[62] K. Raghavachari, G.W. Trucks, J.A. Pople, M. Head-Gordon, Chem. Phys. Lett. 157 (1989) 479.
[63] T.H. Dunning, J. Chem. Phys. 90 (1989) 1007.
[64] M.J. Frisch, G.W. Trucks, H.B. Schlegel, G.E. Scuseria, M.A. Robb, J.R. Cheeseman, V.G. Zakrzewski, J.A. Montgomery Jr., R.E. Stratmann, J.C. Burant, S. Dapprich, J.M. Millam, A.D. Daniels, K.N. Kudin, M.C. Strain, O. Farkas, J. Tomasi, V. Barone, M. Cossi, R. Cammi, B. Mennucci, C. Pomelli, C. Adamo, S. Clifford, J. Ochterski, G.A. Petersson, P.Y. Ayala, Q. Cui, K. Morokuma, D.K. Malick, A.D. Rabuck, K. Raghavachari, J.B. Foresman, J. Cioslowski, J.V. Ortiz, A.G. Baboul, B.B. Stefanov, G. Liu, A. Liashenko, P. Piskorz, I. Komaromi, R. Gomperts, R.L. Martin, D.J. Fox, T. Keith, M.A. Al-Laham, C.Y. Peng, A. Nanayakkara, M. Challacombe, P.M.W. Gill, B. Johnson, W. Chen, M.W. Wong, J.L. Andres, C. Gonzalez, M. Head-Gordon, E.S. Replogle, J.A. Pople, Gaussian 98, Revision A.11, Gaussian, Inc., Pittsburgh, PA, 2001.
[65] T.J. Barton, A. Revis, I.M.T. Davidson, S. Ijadi-Maghsoodi, K.J. Hughes, M.S. Gordon, J. Am. Chem. Soc. 108 (1986) 4022.
[66] K. Komaguchi, Y. Ishiguri, H. Tachikawa, M. Shiotani, Phys. Chem. Chem. Phys. 4 (2002) 5276.
[67] Available from: <http://webbook.nist.gov/chemistry/>.
[68] L. Andrews, X. Wang, J. Phys. Chem. A 106 (2002) 7696.
[69] L. Li, J.T. Graham, W. Weltner, J. Phys. Chem. A 105 (2001) 11018.
[70] N. Legay-Sommaire, F. Legay, J. Phys. Chem. A 102 (1998) 8759.
[71] D.E. Milligan, M.E. Jacox, J. Chem. Phys. 47 (1967) 5146.
[72] Y. Sumiyoshi, K. Tanaka, T. Tanaka, Appl. Surf. Sci. 79/80 (1994) 471.
[73] T.J. Sears et al., J. Chem. Phys. 111 (1999) 9213.
[74] S. Pinchas, I. Laulicht, Infrared Spectra of Labeled Compounds, Academic Press, London, 1971.
[75] R.I. Kaiser, G. Eich, A. Gabrysch, K. Roessler, Astrophys. J. 484 (1997) 487.
[76] D. Drouin, P. Hovington, R. Gauvin, Scanning 19 (1997) 1.
[77] M.B. Coolidge, W.T. Bordon, J. Am. Chem. Soc. 110 (1988) 2298.
[78] W. Thiel, A.A. Voityuk, J. Mol. Struct. (Theochem) 313 (1994) 141.